Journal of Electroanalytical Chemistry 765 (2016) 92–99

Contents lists available at ScienceDirect

Journal of Electroanalytical Chemistry

journal homepage: www.elsevier.com/locate/jelechem

Simulation of interfacial pH changes during hydrogen evolution reaction

Evaldo B. Carneiro-Neto [a,b], Mauro C. Lopes [b], Ernesto C. Pereira [a,*]

[a] LIEC - DQ - Universidade Federal de São Carlos, 13565-905, São Carlos, São Paulo, Brazil
[b] LINE - DEQ - Universidade Estadual do Centro-Oeste, Guarapuava, 85040-080, Paraná, Brazil

ARTICLE INFO

Article history:
Received 16 May 2015
Received in revised form 17 September 2015
Accepted 21 September 2015
Available online 25 September 2015

Keywords:
HER
Volmer-Taffel
Volmer-Heyrovský
Finite elements
Computational electrochemistry

ABSTRACT

This work investigates the possibility of interfacial pH changes during a hydrogen evolution reaction using a finite elements simulation approach. This reaction is a common side step observed in many electrochemical systems, such as electrodeposition or corrosion. To develop a general approach, different mechanisms, i.e., Volmer/Tafel and Volmer/Heyrovský, were investigated. It is observed that for V-H mechanism the interfacial pH change increases 4.2 pH units for those cases where the bulk pH is 5.0. Therefore, in this case, the instant pH at the interface become alkaline, although the bulk is still acidic, which could justify parallel reactions such as metal hydroxide formation in metal electrodeposition. Besides, the interfacial pH changes and the corresponding pH profiles were calculated under several experimental conditions including the composition of the metallic electrode, the bulk solution pH and the total buffer concentration ($[HA]+[A^-]$).

1. Introduction

Interfacial pH change is commonly evoked to explain the hydroxide formation during metal electroplating from acid baths. Indeed, hydroxide formation has been detected in different systems such as cobalt [1–6], zinc [7–9], iron [10], ZnFe [11,12], CoW [13], ZnCo [11,14,15], ZnNi [11], NiCo [16] and FeNi [17] alloys electrodeposition. Due to the high cathodic polarization employed in these experiments, the hydrogen evolution reaction (HER) is an ubiquitous side reaction, inducing a local pH increase at the electrode/electrolyte interface even in those cases the electrolyte is buffered.

Considering the results described above, several electrochemical and non-electrochemical procedures have been tried for the direct measurement of the pH near the electrode surface [18]. Non-electrochemical ones involve the addition of a suitable pH indicator and its detection by optical methods [19,20]. This approach results in averaging pH over a region in front of the electrode, with a thickness depending on the experimental details and spatial resolution of the instrumentation employed. Electrochemical methods involve the placement of a pH sensitive electrode in the vicinity of the working electrode which shields the flux of electroactive species. Indirect measurement with a rotating ring-disk electrode avoids this problem, but requires the solution of diffusion-convection equation in the presence of homogeneous reactions which only in particular cases has an analytical solution. Ohmic drop between the ring and the reference electrode and the adsorption of hydrogen bubbles on the ring are also issues of concern, which, under certain conditions, make these measurements inaccurate. Owing to these inherent experimental difficulties, conflicting results have been reported, as noted by Khun and Chan [18]. From a different point of view, computational experiments are important to support the measured results and to estimate pH changes when an experimental approach is difficult, especially in those cases where the near electrode solution pH has a transient value during the data collection.

In the literature, there are few papers devoted to study this phenomenon from a modeling perspective. A natural approach is to simulate the hydrogen evolution reaction in the absence of metal deposition, before proceeding to the more complicated case of metal and hydrogen co-depositions. Following this approach, Hessami and Tobias [21] calculated the H_3O^+ concentration in the ring as a function of several hydrogen evolution currents applied to the disk in a rotating ring-disk experiment. They developed an approximate analytical solution for the diffusion-convection equation assuming equal diffusivity for OH^- and H_3O^+. A similar approach was adopted by Albery and Calvo [22] but assuming a proton release reaction on the disk. In both papers the details of the interfacial kinetics on the disk are not explicitly considered and a full mass transport control seems to be assumed.

Deslouis et al. [23] used the impinging jet cell method to detect interfacial pH changes during the oxygen reduction reaction. The authors detected changes in the pH up to 5 units, depending on the applied potential range, which are in agreement with the theoretical approach developed in the same paper. A linearized concentration gradient and simplified electrode kinetics were assumed. The pH variation at an oil/water interface was also modeled [24–26].

Considering the importance of HER for many different electrochemical systems and the lack of published papers for experimental conditions which can not be described by analytical solutions of differential

* Corresponding author.
E-mail addresses: evaldoquimica@gmail.com (E.B. Carneiro-Neto), mauro@unicentro.br (M.C. Lopes), ernesto@ufscar.br (E.C. Pereira).

http://dx.doi.org/10.1016/j.jelechem.2015.09.029
1572-6657/

equations, in this work we develop a finite element calculation to simulate different experimental conditions. By the use of the last generation finite element software, a full numerical solution is possible, without oversimplifications and including detailed kinetic formulation for HER. Homogeneous processes are also modeled by a full kinetic formulation without any adiabatic elimination. In this first paper, we describe the one-dimensional plane electrode considering the charge transfer, ionic transport in the solution by diffusion, the cover of the surface by the formed species (using Langmuir isotherm), and the recombination constants of OH^- and H_3O^+. The influence of several experimental conditions such as the nature of metallic electrode, bulk solution pH and the total buffer concentration ($[HA]+[A^-]$) were studied.

2. Theory

In the literature, two main mechanisms have been proposed to describe the HER: Volmer-Tafel (V-T) and Volmer-Heyrovský (V-H) [27–32]. Both mechanisms start with the discharge step (Volmer reaction), described by reaction I in acidic media and reaction (II) in neutral or alkaline media. In the reactions below *s* denotes an active site on the metal surface.

$$H_3O^+_{(aq)} + s + e^- \underset{k_{1,b}}{\overset{k_{1,f}}{\rightleftharpoons}} H_{(ads)} + H_2O_{(l)} \quad (I)$$

$$H_2O_{(l)} + s + e^- \underset{k_{2,b}}{\overset{k_{2,f}}{\rightleftharpoons}} H_{(ads)} + OH^-_{(aq)} \quad (II)$$

In the V-T mechanism, hydrogen evolution occurs by the recombination of two hydrogen atoms adsorbed on metal surface, as described by reaction (III).

$$H_{(ads)} + H_{(ads)} \xrightarrow{k_3} H_{2(g)} + s + s \quad (III)$$

In the V-H mechanism, gaseous hydrogen is formed by electrochemical desorption of H (Heyrovský reaction) as described by reaction IV in acidic media and V in neutral or alkaline media.

$$H_3O^+_{(aq)} + H_{(ads)} + e^- \xrightarrow{k_4} H_{2(g)} + H_2O_{(l)} + s \quad (IV)$$

$$H_2O_{(l)} + H_{(ads)} + e^- \xrightarrow{k_5} H_{2(g)} + OH^-_{(aq)} + s \quad (V)$$

Steps I and IV are the main processes under low negative overpotential and/or bulk solution acidic pH, whereas steps II and V occur in high negativeoverpotential and/or bulk solution alkaline pH. It is worth to mention that different steps can occur at the same time depending on the experimental conditions.

Besides it is important to consider the water auto-ionization which can also affect the interfacial pH:

$$H_3O^+_{(aq)} + OH^-_{(aq)} \underset{k_{w,b}}{\overset{k_{w,f}}{\rightleftharpoons}} 2H_2O_{(l)} \quad (VI)$$

Finally, in those media where a buffer solution is used to inhibit the pH change, the following reaction must be considered:

$$HA_{(aq)} + H_2O_{(l)} \underset{k_{a,b}}{\overset{k_{a,f}}{\rightleftharpoons}} H_3O^+_{(aq)} + A^-_{(aq)} \quad (VII)$$

Steps I and II are assumed to be faster than the others in both mechanisms. Saraby and Reintjes, using Volcano plots, proposed that V-T mechanism must be used for materials with high adsorption energy of H atoms, whereas V-H mechanism occurs where the surface has low adsorption energy of H atoms [33,34]. The HER's exchange current density are reported in a widely range which spans from 10^{-10}A·cm^{-2} to 10^{-2}A·cm^{-2}. This large variation could be associated to the changes in the mechanism of the reaction coming from different experimental conditions as, for example, the pH of the solution and surface material composition [31].

In this work, we assume a planar disk electrode whose radius is much larger than the diffusion layer, so that the mass transport in solution can be considered linear. Consequently, the model is valid in a 1D domain as presented in Fig. 1.

To obtain a general solution for the physicochemical model it was used dimensionless variables in agreement to those relationships suggested by Britz [35] which will be used in the description of the next equations. The transformation are described in Table 1.

The model assumes that the ion transport is described only by the diffusion term of the Nernst-Planck equation which is reasonable for those experimental situations where a supporting electrolyte is used. Besides, the homogeneous reaction due to auto-ionization (reaction VI) and the buffer effect (reaction VII) are also considered. Therefore, the concentration of H_3O^+ follows the diffusion–reaction equation:

$$\frac{\partial C_{H_3O^+}}{\partial \tau} = \frac{\partial^2 C_{H_3O^+}}{\partial X^2} + K_{w,f} - K_{w,b} C_{OH^-} C_{H_3O^+} + K_{a,f} C_{HA} - K_{a,b} C_{A^-} C_{H_3O^+} \quad (1)$$

Similarly, for OH^- we write:

$$\frac{\partial C_{OH^-}}{\partial \tau} = \hat{D}_{OH^-} \frac{\partial^2 C_{OH^-}}{\partial X^2} + K_{w,f} - K_{w,b} C_{OH^-} C_{H_3O^+} \quad (2)$$

Finally, when the solution is buffered, two other equations must be used to describe the transient concentration of HA and A^-:

$$\frac{\partial C_{HA}}{\partial \tau} = \frac{\partial^2 C_{HA}}{\partial X^2} - K_{a,f} C_{HA} + K_{a,b} C_{A^-} C_{H_3O^+} \quad (3)$$

and

$$\frac{\partial C_{A^-}}{\partial \tau} = \frac{\partial^2 C_{A^-}}{\partial X^2} + K_{a,f} C_{HA} - K_{a,b} C_{A^-} C_{H_3O^+} \quad (4)$$

At the start of the experiment, the concentration of all the species are uniform throughout the solution. So, the following initial condition apply:

$$C_{H_3O^+} = 1, \quad C_{OH^-} = \frac{K_{w,f}}{K_{w,b}}, \quad C_{HA} = C^*_{HA}, \quad C_{A^-} = C^*_{A^-}, \quad (5)$$
$$\tau = 0 \wedge X \geq 0$$

At the end of the diffusion layer, it was used the semi-infinite diffusion conditions:

$$C_{H_3O^+} = 1, \quad C_{OH^-} = \frac{K_{w,f}}{K_{w,b}}, \quad C_{HA} = C^*_{HA}, \quad (6)$$
$$C_{A^-} = C^*_{A^-}, \quad X \to \infty \wedge \tau \geq 0$$

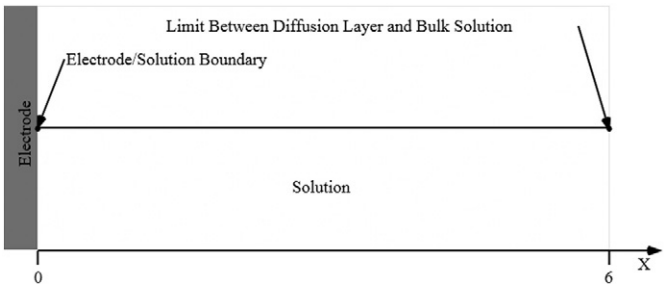

Fig. 1. 1D geometry scheme.

Table 1
Dimensionless variables.

Variable	Definition	Dimensionless parameters
Dimensionless concentration	$C_i = \frac{[i]}{[H_3O^+]^*}$	$[i]$ is the bulk molar concentration of specie i, $[H_3O^+]^*$ is the bulk hydronium concentration
Dimensionless time	$\tau = \frac{t}{t_{total}}$	t is the time in seconds and t_{total} is the total time
Dimensionless space	$X = \frac{x}{\delta}$, $\delta = \sqrt{D_{H_3O^+} t_{total}}$	x is the distance from electrode; $D_{H_3O^+}$ is the hydronium diffusion coefficient
Dimensionless diffusion coefficient	$\hat{D}_i = \frac{D_i}{D_{H_3O^+}}$	
Dimensionless surface concentration	$\Gamma_{ad} = \frac{\gamma}{[H_3O^+]^* \delta}$	γ=dimensional surface concentration
Dimensionless potential	$\phi = fE$	$f = \frac{F}{RT}$; F= Faraday constant; R= ideal gas constant; T= temperature; E= electric potential
Dimensionless current	$\chi = \frac{j\delta}{nFD_{H_3O^+} A[H_3O^+]^*}$	j= dimensional current; n= number of transferred electrons; A= electrode surface area

The boundary conditions at the electrode/solution interface are provided by the interfacial reactions I-V which determines the concentration gradients (fluxes) of the involved species at $X=0$. In V-T mechanism, the hydronium ion participates only in the step I. Consequently, the boundary condition for H_3O^+ is:

$$\left(\frac{\partial C_{H_3O^+}}{\partial X}\right)_{X=0} = \Gamma_{max} K_{1,b} \theta e^{(1-\alpha)(\phi_{applied}-\phi_1)} - \Gamma_{max} K_{1,f} C_{H_3O^+} (1-\theta) e^{-\alpha(\phi_{applied}-\phi_1)}, \quad \tau > 0 \tag{7}$$

Analogously for OH^-:

$$\hat{D}_{OH^-}\left(\frac{\partial C_{OH^-}}{\partial X}\right)_{X=0} = \Gamma_{max} K_{2,f} (1-\theta) e^{-\alpha(\phi_{applied}-\phi_2)} - \Gamma_{max} K_{2,b} C_{OH^-} \theta e^{(1-\alpha)(\phi_{applied}-\phi_2)}, \quad \tau > 0 \tag{8}$$

Once the above equations depends on the surface coverage (θ), an additional ordinary differential equation is required to determine it:

$$\frac{d\theta}{d\tau} = (1-\theta)\left[K_{1,f} C_{H_3O^+} e^{-\alpha(\phi_{applied}-\phi_1)} + K_{2,f} e^{-\alpha(\phi_{applied}-\phi_2)}\right] + \theta\left[-K_{1,b} e^{(1-\alpha)(\phi_{applied}-\phi_1)} - K_{2,b} e^{(1-\alpha)(\phi_{applied}-\phi_2)}\right] - K_3 \Gamma_{max} \theta^2, \quad \tau > 0 \tag{9}$$

In V-H mechanism, H_3O^+ participates in steps I and IV while OH^- participates in steps II and V, leading to the following boundary conditions:

$$\left(\frac{\partial C_{H_3O^+}}{\partial X}\right)_{X=0} = \Gamma_{max} K_{1,b} \theta e^{(1-\alpha)(\phi_{applied}-\phi_1)} - \Gamma_{max} K_{1,f} (1-\theta) C_{H_3O^+} e^{-\alpha(\phi_{applied}-\phi_1)} + \Gamma_{max} K_4 \theta C_{H_3O^+} e^{-\alpha(\phi_{applied}-\phi_4)}, \quad \tau > 0 \tag{10}$$

$$\hat{D}_{OH^-}\left(\frac{\partial C_{OH^-}}{\partial X}\right)_{X=0} = \Gamma_{max} K_{2,f} (1-\theta) e^{-\alpha(\phi_{applied}-\phi_2)} + \Gamma_{max} K_5 \theta e^{-\alpha(\phi_{applied}-\phi_5)} - \Gamma_{max} K_{2,b} \theta C_{OH^-} e^{(1-\alpha)(\phi_{applied}-\phi_2)}, \quad \tau > 0 \tag{11}$$

In this case, the surface coverage follows:

$$\frac{d\theta}{d\tau} = (1-\theta)\left[K_{1,f} C_{H_3O+} e^{-\alpha(\phi_{applied}-\phi_1)} + K_{2,f} e^{-\alpha(\phi_{applied}-\phi_2)}\right] + \theta\left[-K_4 C_{H_3O+} e^{-\alpha(\phi_{applied}-\phi_4)} - K_5 e^{-\alpha(\phi_{applied}-\phi_5)}\right] + \theta\left[-K_{1,b} e^{(1-\alpha)(\phi_{applied}-\phi_1)} - K_{2,b} C_{OH^-} e^{(1-\alpha)(\phi_{applied}-\phi_2)}\right], \quad \tau > 0 \tag{12}$$

Both Eqs. (9) and (12) are subjected to the initial condition:

$$\frac{d\theta}{d\tau} = 0, \quad \tau = 0 \tag{13}$$

The non-electroactive species have a null flux near the electrode, and, therefore:

$$\hat{D}_{HA}\left(\frac{\partial C_{HA}}{\partial X}\right)_{X=0} = 0 \quad \text{and} \quad \hat{D}_{A^-}\left(\frac{\partial C_{A^-}}{\partial X}\right)_{X=0} = 0 \tag{14}$$

The current is evaluated by the gradient of electroactive species at the electrode/solution interface. It is instructive to express the total current as the sum of two terms associated with hydronium and water reduction, respectively:

$$\chi_{H_3O^+} = -\left(\frac{\partial C_{H_3O^+}}{\partial X}\right)_{X=0} \tag{15}$$

$$\chi_{OH^-} = \hat{D}_{OH^-}\left(\frac{\partial C_{OH^-}}{\partial X}\right)_{X=0} \tag{16}$$

$$\chi_F = \chi_{H_3O^+} + \chi_{OH^-} \tag{17}$$

The set of equations presented above are general to fit ever experimental conditions generally found in the literature except those ones where it is necessary to consider the transport by convection and/or migration. In this last case, it is easy to include such effects in the equation setup, but, experimentally, it is not important in those case where the solution in the electrochemical cell includes a supporting electrolyte. It is important to stress out that the interfacial pH, $\Delta pH_{e|s}$, is defined as instantaneous pH at zero distance from the electrode, according to:

$$\Delta pH_{e|s} = -\log\left(C_{H_3O^+}\right)_{X=0} = -\log\left(\frac{[H_3O^+]}{[H_3O^+]^*}\right)_{X=0} = pH_{X=0} - pH^* \tag{18}$$

The equation above implicitly assumes an ideal solution, since concentrations instead of activities were used. This assumptions is reasonable for the pH range (4–10) dealt in this work, once the H_3O^+ concentration was always below 10^{-4}M.

The final model requires the input of several non-dimensional parameters listed in Tables 2 and 3. Some values used for these parameters are also listed in the tables. If not explicitly stated otherwise, the simulations are performed with these set of parameters values. Table 2 groups the parameters which express rate constants of reactions I to VII. The values of homogeneous rate constants were obtained directly from the literature. The values of heterogeneous rate constants are deduced from exchange current density measurements, assuming that reaction III is the limiting step for V-T mechanism and reaction IV/V is the limiting step for V-H mechanism.

Table 2
Dimensionless constants definitions and base values attributed.

Dimensionless parameter	Value	Definition	Dimensional parameters
K_{1f}	0.3	$k_{1f}antilog(-pH)t_{total}$	k_{1f} = Forward rate constant of step (I)*
K_{1b}	0.015	$k_{1b}t_{total}$	k_{1b} = Backward rate constant of step (I)*
K_{2f}	0.03	$k_{2f}t_{total}$	k_{2f} = Forward rate constant of step (II)*
K_{2b}	0.015	$k_{2b}antilog(-pH)t_{total}$	k_{2b} = Backward rate constant of step (II)*
K_3	$1\ 10^7$	$k_3antilog(-pH)t_{total}$	k_3 = Forward rate constant of step (III)*
K_4	0.1	k_4t_{total}	k_4 = Forward rate constant of step (IV)*
K_5	0.1	$2\ k_5antilog(-pH)\delta t_{total}$	k_5 = Forward rate constant of step (V)*
$K_{w,f}$	$4.333\ 10^3$	$\frac{k_{w,f}t_{total}}{antilog(-pH)}$	$k_{w,f}$ = Forward rate constant of auto-ionization of water**
$K_{w,b}$	$4.2\ 10^7$	$k_{w,b}antilog(-pH)t_{total}$	$k_{w,b}$ = Backward rate constant of auto-ionization of water**
$K_{a,f}$	−***	$k_{a,f}t_{total}$	$k_{a,f}$ = Forward rate constant of step (VII)**
$K_{a,b}$	−***	$k_{a,b}antilog(-pH)t_{total}$	$k_{a,b}$ = Backward rate constant of step (VII)**

* values deduced from [31,36,37].
** values obtained from [38].
*** because initially without buffer.

3. Methods

The set of equations was solved by the finite element methods using COMSOL Multiphysics 4.0a software. The commercial finite element software allows the use of the most robust numerical techniques without the need to write computer codes. COMSOL Multiphysics is a very popular package in the electrochemical community and proved to be very effective, provided that an appropriate mesh is used [42,43]. The calculation were performed using a personal computer with Intel i7 processor with 24 GB of RAM in a Ubuntu Linux 10.04 operational system. We developed the model described above in a 1D geometry which means that it is possible to simulate a plane electrode disregarding boundary effects. The details about the numerical strategies and convergence criteria can be found in the COMSOL report added as supplementary material. In short, the mesh consists of 3535 nodes, and near to the electrode surface each element has the size of 10^{-6}. The relative tolerance was chosen to be 10^{-7}. The linear system of equations was solved using a direct method with the solver PARDISO. Although the simulations were performed using dimensionless unities for generality, the solution pH initially considered was 5.0. We choose this value because it is very common in many experimental situations and, in these cases, solution buffers are also commonly used. For the investigation of the effect of the buffer total concentration, a bulk solution pH of 4.75 was used as consequence of the equilibrium constant of the sodium acetate/acetic acid physicochemical parameters used in the calculations.

Table 3
Dimensionless parameters set in one-dimensional simulations.

Parameter	Value	Description
$D_{H_3O^+}$	1	Dimensionless hydronium diffusion coefficient*
D_{OH^-}	0.5663	Dimensionless hydroxile diffusion coefficient*
D_{HA}	0.138546	Dimensionless acid diffusion coefficient*
D_{A^-}	0.116958	Dimensionless conjugate base diffusion coefficient*
ϕ_1	6.7	Dimensionless formal potential of step (I)**
ϕ_2	−15.5	Dimensionless formal potential of step (II)**
ϕ_4	0	Dimensionless formal potential of step (IV)*
ϕ_5	−32	Dimensionless formal potential of step (V)*
$C^*_{H_3O^+}$	1	Dimensionless hydronium bulk concentration
$C^*_{OH^-}$	$\frac{K_{w,f}}{K_{w,b}}$	Dimensionless hydroxile bulk concentration
C^*_{HA}	0	Dimensionless acid bulk concentration
$C^*_{A^-}$	0	Dimensionless conjugate base bulk concentration
Γ_{max}	$1.882\ 10^{-4}$	Dimensionless maximum concentration of adsorbate***
α	0.5	Transfer coefficient
v_{ad}	60	Dimensionless sweep rate
ϕ_0	20	Dimensionless initial potential

* values taken from the CRC Handbook of Chemistry and Physics [39].
** deduced from voltammograms in [40].
*** [41].

4. Results and discussion

Fig. 2 presents the non-dimensional current density (upper) and pH change (lower) as a function of potential for both Volmer-Tafel (left) and Volmer-Heyrovský (right) mechanisms. Each graph in the Fig. 2 shows three curves simulated with different values for the rate constant of the determining step, reaction III for V-T mechanism and reaction IV for V-H mechanism. Considering the curves represented by solid lines, it is observed that, in the V-T mechanism, the current decrease down to a limit value which is an expected result once the reaction is limited by the Tafel step for high coverage level. At the onset of the cathodic wave, −0.1 *V*, the pH starts to change and increases until to the end of the sweep with $\Delta pH_{e|s}$ reaching the final value of 0.14 pH units. For V-H mechanism the onset of the cathodic wave occurs at −0.35 V and the current density is much larger, showing a peak which indicates the mass transport limitation. Consequently, the pH change is more significant reaching a final value of 4.2 pH units. Although a current peak in HER is not commonly observed, there are several papers in the literature which described such characteristic point especially for intermediate values of solution pH which are, as described in the method section, used in this work [36,44]. The presence or absence of peak is determined by the relative contributions of water reduction, steps II or V, and hydronium reduction, steps I or IV. This aspect will be further investigated in this work.

The pH variation is obviously determined by the interplay between the consumption of hydronium ions at the electrode/solution interface, due to interfacial reactions, and the replenishment of hydronium ions, owing to diffusion flux towards the electrode surface. In the case of V-T mechanism, the sluggish kinetics is readily compensated by the diffusion and the pH change is low. However, at the end of the experiment, the pH is still increasing, which means that although the reaction is limited by the degree of coverage at the interface, the mass transport towards and away from this point has not reached steady state. Obviously, in the case of V-H mechanism, the system is far from steady state.

It is important to mention that, for simulations shown in Fig. 2, the chosen values for the rate constants yield a global rate compatible with experimental values reported for those metals where each mechanism is expected. Hence, for V-T mechanism the exchange current density is in the order of $10^{-9}A{\cdot}cm^{-2}$ (solid lines), consistently with the values reported for metals with high H adsorption energy, such as Hg and Pb. In the case of V-H mechanism, the exchange current density is four orders of magnitude higher, as reported for transition metals like Ni and Co. For these metals, the H adsorption energy is low, which assures that $E^0_V = -E^0_H \approx 0$. The proximity of these standard potentials makes possible the appearance of an adsorption pre-peak before the hydrogen evolution wave, as reported in the literature. This subtle characteristic was also detected by our model and it is presented in the inset of upper-right graph in Fig. 2.

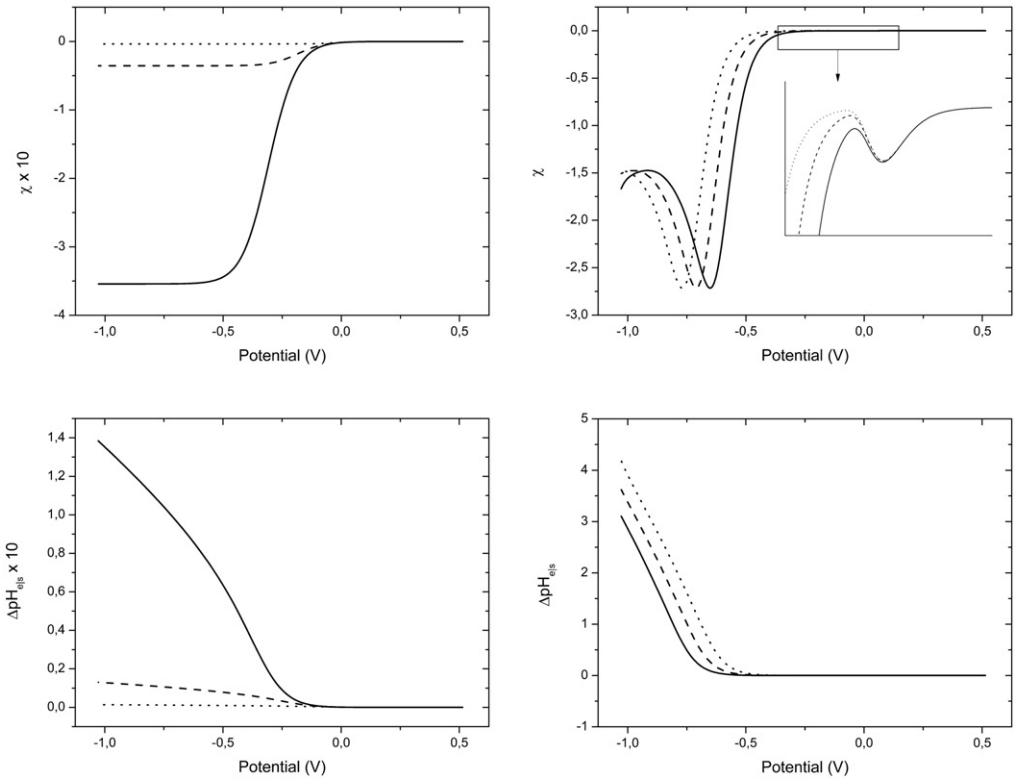

Fig. 2. Non-dimensional current density (upper) and pH changes (lower) as a function of potential simulated for V-T (left) and V-H (right) mechanisms using several rate constants for determining steps: $K_3 = 1 \times 10^7$ (solid line), $K_3 = 1 \times 10^6$ (dashed line) and $K_3 = 1 \times 10^5$ (dotted line) in the left. $K_4 = 0.1$ (solid line), $K_4 = 0.0316$ (dashed line) and $K_4 = 0.01$ (dotted line) in the right.

From the discussion above, one can conclude that for those cases where the V-T mechanism occurs the interfacial pH changes are low and, consequently, more difficult to be experimentally detected. Even though, this not preclude its interference in some parallel reaction at the electrode surface. The situation is completely different for the Volmer-Heyrovský mechanism where the final $\Delta pH_{e|s}$ are up to 4.2 pH units, depending on the value of K_4 in reaction IV. This pH change is very important and can explain different results described in the literature as, for example, the formation of $Co(OH)_2$ proposed to be formed during the electrodeposition of cobalt in solution with pH near 5.0 [3, 4]. In that work, the authors concluded unambiguously the formation of $Co(OH)_2$ from EQCM data.

A point of great relevance is the variation of the heterogeneous reaction rate which occurs when the electrode material is changed. Within the group of metals for which the HER occurs via V-H mechanism, a considerable variation of the exchange current occurs. Consequently a change of the electrode material can lead to different pH variation. The effect of these changes can be simulated by the variation of the rate constant of the step IV, K_4, which is the controlling step for V-H mechanism. Analogously, in the case of V-T mechanism, the effect of the nature of electrode material can be simulated by the variation of the rate constant of the step III. As can be observed in Fig. 2, the higher the rate constant, the greater is the pH variation, as expected. Nevertheless, it is interesting to note the different behavior of the two mechanisms. In the V-T mechanism, the increase of K_3 lead to the increase in the limit current density. In V-H mechanism, when K_4 increases the current curves displace to less negative potentials. A close inspection of the curves shows that, at the current peak, the pH change is the same for the three curves. This means that for the highest value of K_4 studied, the $\Delta pH_{e|s}$ is larger just because the pH changes starts at a more positive potential. Otherwise, it is important to stress out that it was clear, from the computational experiments, that this is an obvious results related to the starting point of the reaction rather than any other more complex mechanistic explanation.

Considering that the most important $\Delta pH_{e|s}$ occurs under V-H mechanism, in the following text we present only the results simulated for this pathway.

Another experimental issue about HER occurs in those cases where the main electroactive specie changes from H_3O^+ to H_2O which occurs in solutions with intermediary pH values. To illustrate this point, Fig. 3 presents the current contributions of water and hydronium separately. The current of hydronium ion reduction predominates throughout the process, even after the current peak. The water reduction becomes

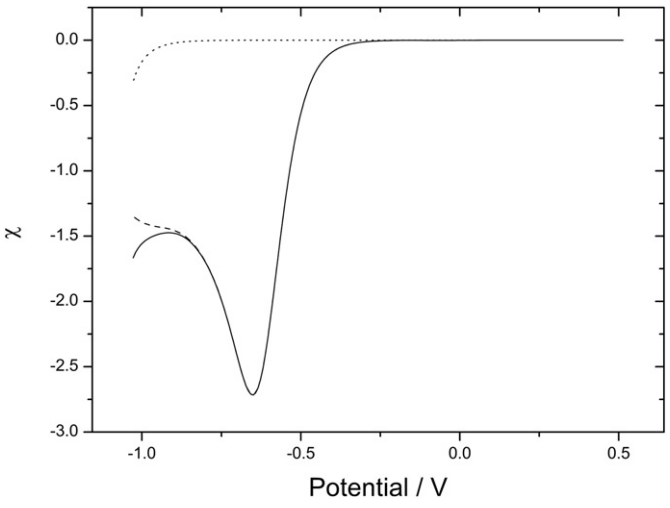

Fig. 3. Decoupling of the total hydrogen evolution current density (solid line) in its components: water reduction (dotted line) and hydronium reduction (dashed line).

important only for very negative potential in the region where the current start to grow again after the peak which is related to the drastic decrease in the concentration of hydronium ions at the interface.

The presence of the peak in the hydrogen evolution reaction only for intermediate pH can be rationalized in terms of the relative contributions of water and hydronium reduction. When the decrease in the hydronium reduction current is compensated by the increase of water reduction current, the peak is not formed. This situation can occur in alkaline pH due to the low hydronium concentration and strong acid pH because, in this case, the decrease of hydronium reduction current occurs only at very negative potential where water reduction is favored.

In Fig. 4, the effect of different bulk solution pHs values are presented for those situation where the pH bulk solution differs by 1 unit. Because dimensionless rate constants are defined as a function of the bulk pH, their values need to be calculated in each pH as presented in Table 4. Once the non-dimensional current is also defined as a function of the bulk pH, we can not compare the non-dimensional current in two different pH's. Therefore, after non-dimensional simulations we recalculate the dimensional values of the current density which are presented in Fig. 3.

For the higher pH, the current density is lower owing to the smaller supply of hydronium ions at the interface. However, a more significant contribution of water reduction is evidenced by the change of the slope of the current curve after the peak. As mentioned above, the increase of water reduction current compensates the decrease of hydronium reduction current, making the peak less defined. Both pH curves are overlaid until the potential value of −0.67 V. Starting from this point they differ and the curve with higher bulk pH has a slightly lower $\Delta pH_{e|s}$.

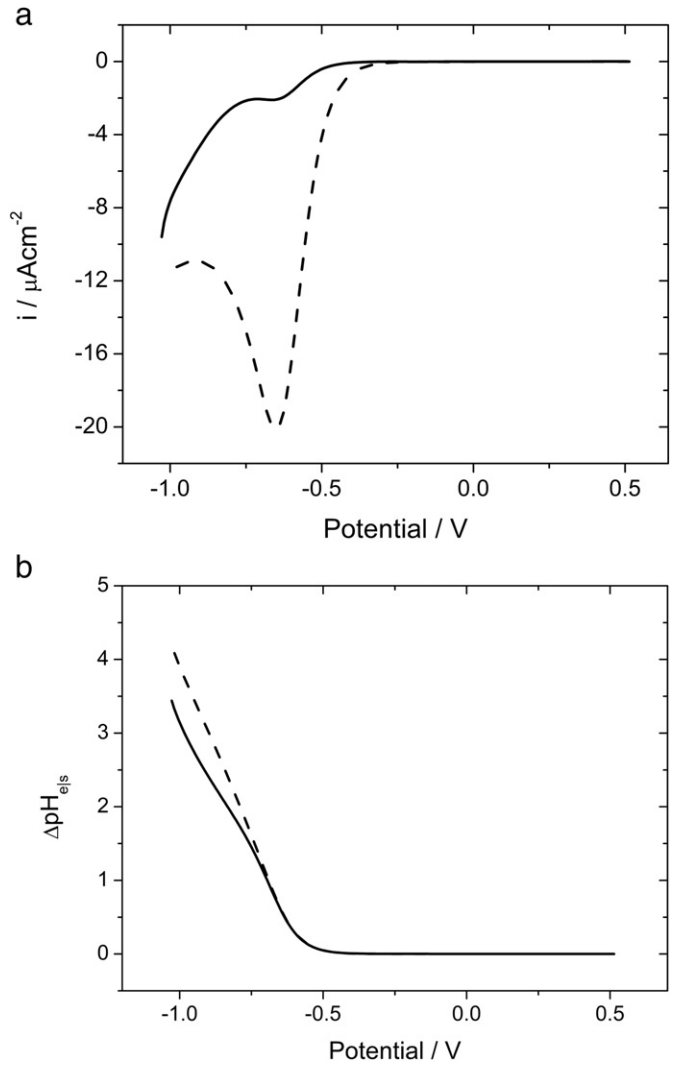

Fig. 4. Effect of bulk pH in the current (upper) and pH change (lower) simulated for V-H mechanism with parameters described in Table 4.

Table 4
Dimensionless constants used in the simulations to compare the voltammetric behavior at two different pHs.

Parameters	pH_1	$pH_2 = pH_1 + 1$
$K_{w,f}$	$4.333\ 10^3$	$4.333\ 10^4$
$K_{w,b}$	$4.2\ 10^7$	$4.2\ 10^6$
K_{1f}	0.3	0.03
K_{2b}	0.015	0.0015
K_3	10^7	10^6
K_4	0.1	0.01
Γ_{ad}	$1.882\ 10^{-4}$	$1.882\ 10^{-3}$

To simulate the pH variation in the presence of a buffer we choose the pH 4.75 (corresponding to an equimolar acetic acid-sodium acetate buffer solution), then some constants had their values changed in agreement with the dimensionless model, which are presented in Table 5.

The results presented in Fig. 5 shows that even in the case of buffer addition, important $\Delta pH_{e|s}$ could occur. In this Figure, the effect of increasing total buffer concentration is presented. It is shown that in the presence of a buffer with total concentration 200 times larger than the hydronium concentration, the changes in pH are attenuated but a change in interfacial pH in the order of 2 pH units is still observed. Once the rate constants for the acid dissociation and anion hydrolysis are very large, we can conclude that the inefficacy of the buffer is associated with the depletion of acid molecules and accumulation of anions at the interface.

It is very important to analyze the extension of the depletion layer of hydronium ions towards the solution, as shown in the lower graph in Fig. 5. First, it is important to note that in all cases the depletion layer extends to a fraction of millimeters towards the solution, being, therefore, much larger than the electric double layer at the interface. This means that any electroactive specie that approximates to the electrode will sense this pH variation. Second, is evident that the higher the total buffer concentration, the narrow is the depletion layer. This shows that the buffer operates not only attenuating the interfacial pH change but also limiting its extension in the solution. The extension of the depletion layer is also important to discuss the measurability of the pH changes. While in our model we treat the pH as a point continuous variable, it is obvious that pH only can be measured by a sensor with a finite dimension. In this sense, knowing the extension of the depletion layer is important to guide experimental measurements.

The simulation here developed investigated several important characteristics of HER which is, generally, found in many experimental measurements. We hope that this approach can help experimentalist to explain some of their results, such as, the one which motivates this work which is the formation of $Co(OH)_2$ during the electrodeposition of cobalt in acid media [3,4].

Table 5
Dimensionless constants used in the simulation for comparing the voltammetric behavior in different concentrations of buffering agents.

Parameters	Values
$K_{w,f}$	1218.74
$K_{w,b}$	$3.733\ 10^7$
K_{1f}	0.2667
K_{2b}	0.02667
K_3	0.0889
$K_{a,f}$	$1.2\ 10^7$
$K_{a,b}$	$1.2\ 10^7$

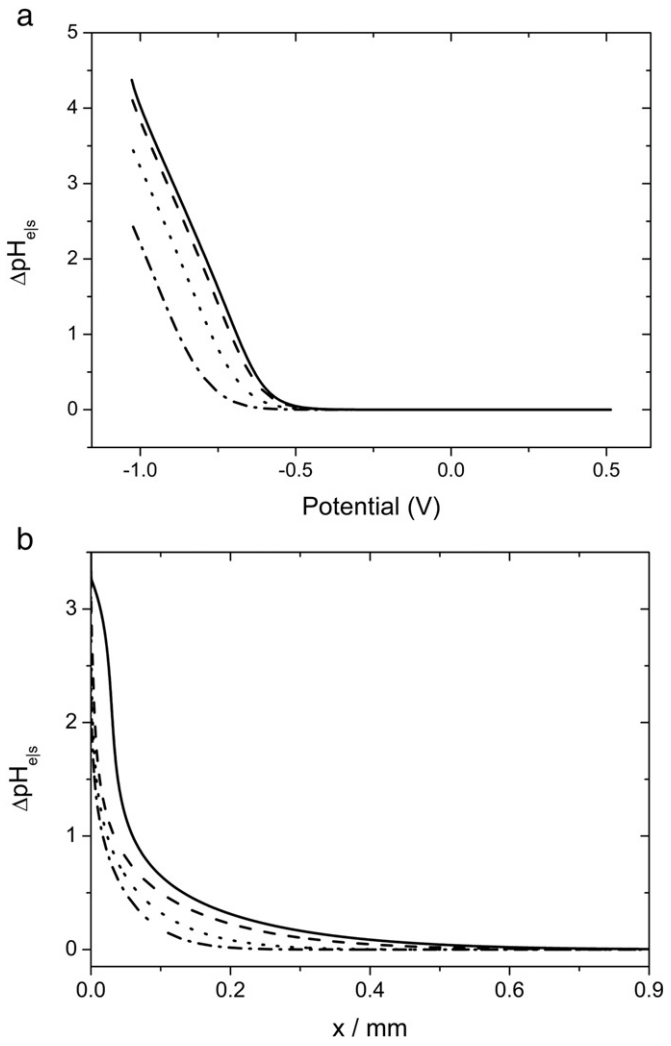

Fig. 5. Variation of pH as a function of potential (upper) and distance from the electrode (lower) in the absence (solid line) and in the presence of buffer solutions with the same pH and different total buffer concentration ([HA] + [A⁻]): 2 (dashed line), 20 (dotted line) and 200 (dash-dotted line).

5. Conclusions

From what has been presented, it can be stated that the interfacial pH changes and, depending on the boundary conditions, this change can reach some units of pH, for the case of the Volmer-Heyrovský mechanism, which is used to describe interfaces which have greater ease to evolve hydrogen. For the case of Volmer-Tafel mechanism, this change was less pronounced because the HER is slower than in V-H, however still it happens. These changes are reflected in an experimental problem that can not be bypassed even in the presence of buffering agents aplenty.

Acknowledgments

The authors want to acknowledge to FAPESP (Grant 2013/07296-2), CNPq and CAPES for financial support.

Appendix A. Supplementary data

Supplementary data to this article can be found online at http://dx.doi.org/10.1016/j.jelechem.2015.09.029.

References

[1] M. Jeffrey, W. Choo, P. Breuer, The effect of additives and impurities on the cobalt electrowinning process, Miner. Eng. 13 (12) (2000) 1231–1241.
[2] J. Matsushima, F. Trivinhostrixino, E. Pereira, Investigation of cobalt deposition using the electrochemical quartz crystal microbalance, Electrochim. Acta 51 (10) (2006) 1960–1966.
[3] J. Santos, R. Matos, F. Trivinhostrixino, E. Pereira, Effect of temperature on Co electrodeposition in the presence of boric acid, Electrochim. Acta 53 (2) (2007) 644–649.
[4] J. Santos, F. Trivinho-Strixino, E. Pereira, Investigation of Co(OH)2 formation during cobalt electrodeposition using a chemometric procedure, Surf. Coat. Technol. 205 (7) (2010) 2585–2589.
[5] A. Franczak, A. Levesque, F. Bohr, J. Douglade, J.-P. Chopart, Structural and morphological modifications of the Co-thin films caused by magnetic field and pH variation, Appl. Surf. Sci. 258 (22) (2012) 8683–8688.
[6] W. Tan, M. Hasnat, N.H.M. Ramalan, W. Soh, N. Mohamed, Influence of flow rates on the electrogenerative Co^{2+} recovery at a reticulated vitreous carbon cathode, Chem. Eng. J. 189-190 (2012) 182–187.
[7] K. Raeissi, A. Saatchi, M. Golozar, Effect of nucleation mode on the morphology and texture of electrodeposited zinc, J. Appl. Electrochem. (2003) 635–642.
[8] A. Gomes, M. da Silva Pereira, Pulsed electrodeposition of Zn in the presence of surfactants, Electrochim. Acta 51 (7) (2006) 1342–1350.
[9] R.C.M. Salles, G.C.G. de Oliveira, S.L. Díaz, O.E. Barcia, O.R. Mattos, Electrodeposition of Zn in acid sulphate solutions: pH effects, Electrochimica Acta 56 (23) (2011) 7931–7939, http://dx.doi.org/10.1016/j.electacta.2010.12.026.
[10] S. Daz, J. Calderón, O. Barcia, O. Mattos, Electrodeposition of iron in sulphate solutions, Electrochim. Acta 53 (25) (2008) 7426–7435.
[11] H. Fukushima, T. Akiyama, M. Yano, T. Ishikawa, R. Kammel, Electrodeposition behavior of Zn-Iron-group metal alloys from sulfate and chloride baths, ISIJ Int. 33 (9) (1993) 1009–1015.
[12] S. Daz, ZnFe anomalous electrodeposition: stationaries and local pH measurements, Electrochim. Acta 47 (25) (2002) 4091–4100.
[13] S.S. Belevskii, H. Cesiulis, N.I. Tsyntsaru, a.I. Dikusar, The role of mass transfer in the formation of the composition and structure of CoW coatings electrodeposited from citrate solutions, Surf. Eng. Appl. Electrochem. 46 (6) (2011) 570–578.
[14] K. Higashi, H. Fukushima, T. Urakawa, T. Adaniya, K. Matsudo, Mechanism of the electrodeposition of zinc alloys containing a small amount of cobalt, J. Electrochem. Soc. 128 (10) (1981) 2081–2085, http://dx.doi.org/10.1149/1.2127194.
[15] E. Gómez, E. Vallés, Electrodeposition of zinc + cobalt alloys: inhibitory effect of zinc with convection and pH of solution, J. Electroanal. Chem. 397 (1995) 177–184.
[16] C. Lupi, D. Pilone, Electrodeposition of nickel-cobalt alloys: the effect of process parameters on energy consumption, Miner. Eng. 6875 (01) (2001) 1403–1410.
[17] H. Nakano, M. Matsuno, S. Oue, M. Yano, S. Kobayashi, H. Fukushima, Mechanism of anomalous type electrodeposition of Fe-Ni alloys from sulfate solutions, Mater. Trans. 45 (11) (2004) 3130–3135.
[18] A.T. Khun, C.Y. Chan, pH changes at near-electrode surfaces, J. Appl. Electrochem. 13 (1983) 189–207.
[19] S. Cannan, I.D. Macklam, P.R. Unwin, Three-dimensional imaging of proton gradients at microelectrodes surfaces using confocal laser scanning microscopy, Electrochem. Commun. 4 (2002) 886–892.
[20] N.C. Rudd, S. Cannan, E. Bitziou, I. Ciani, A.L. Whitworth, P.R. Unwin, Fluorescence confocal laser scanning microscopu as a probe of ph gradients in electrode reactions and surface activity, Anal. Chem. 77 (2005) 6205–6217.
[21] S. Hessami, C.W. Tobias, In-situ measurement of interfacial pH using a rotating ring-disk electrode, AICHE J. 39 (1) (1993) 149–162.
[22] W.J. Albery, E.J. Calvo, Ring-disc electrodes. Part 21.-pH measurement with the ring, J. Chem. Soc. Faraday Trans. 1 79 (11) (1983) 2583–2596.
[23] C. Deslouis, I. Frateur, G. Maurin, B. Tribollet, Interfacial pH measurement during the reduction of dissolved oxygen in a submerged impinging jet cell, J. Appl. Electrochem. 27 (4) (1997) 482–492.
[24] S.A. Dassie, Effect of ligand protoproton on the facilitated ion transfer across oil/water interfaces. ii. complex formation, J. Electroanal. Chem. 585 (2005) 256–268.
[25] S.A. Dassie, Effect of ligand protoproton on the facilitated ion transfer reactions across oil/water interfaces. i. water autoprotolysis, J. Electroanal. Chem. 578 (2005) 159–170.
[26] J.I. Garcia, M.B. Oviedo, S.A. Dassie, Effect of ligand protonation on the facilitated ion transfer reactions across oil/water interfaces. iv. buffer solution effect, J. Electroanal. Chem. 645 (2010) 1–9.
[27] J.O. Bockris, I. Ammar, A. Huq, The mechanism of the hydrogen evolution reaction on platinum, silver and tungsten surfaces in acid solutions, J. Phys. Chem. 61 (7) (1957) 879–886.
[28] M. Devanathan, M. Selvaratnam, Mechanism of the hydrogen-evolution reaction on nickel in alkaline solutions by the determination of the degree of coverage, Trans. Faraday Soc. 56 (1960) 1820–1831.
[29] J. Bockris, A. Reddy, Modern electrochemistry, vol. 2, Macdonald, London 1970, pp. 1231–1251.
[30] A.J. Bard, L.R. Faulkner, Electrochemical methods fundamentals and applications, Wiley, New York, 2001.
[31] V. Bagotsky, Fundamentals of electrochemistry, Wiley-Interscience, 2006.
[32] Y.F. Cheng, L. Niu, Mechanism for hydrogen evolution reaction on pipeline steel in near-neutral pH solution, Electrochem. Commun. 9 (2007) 558–562.
[33] A. Saraby-Reintjes, The hydrogen evolution reaction under mixed kinetic control, J. Chem. Soc. Faraday Trans. 1 82 (11) (1986) 3343–3355.
[34] A. Saraby-Reintjes, Kinetic criteria for the mechanism of the hydrogen evolution reaction, Electrochim. Acta 31 (2) (1986) 251–254.
[35] D. Britz, Digital simulation in electrochemistry, Springer-Verlag New York Inc., 2005

[36] S. Chen, A. Kucernak, Electrodeposition of platinum on nanometer-sized carbon electrodes, J. Phys. Chem. B 107 (33) (2003) 8392–8402.
[37] D. Tang, J. Lu, L. Zhuang, P. Liu, Calculations of the exchange current density for hydrogen electrode reactions: A short review and a new equation, J. Electroanal. Chem. 644 (2) (2010) 144–149.
[38] G.G. Hammes, Very fast reactions in solution, Science 151 (3717) (1966) 1507–15011.
[39] D.R. Lide, CRC Handbook of Chemistry and Physics, 85th ed., vol. 85, CRC press, Boca Raton, FL, 2005.
[40] D. Pletcher, S. Sotiropoulos, Hydrogen adsorption-desorption and oxide formation-reduction on polycrystalline platinum in unbuffered aqueous solutions, Journal of the Chemical Society, Faraday Trans. 90 (24) (1994) 3663.
[41] V. Santos, G. Tremiliosi Filho, Correlação entre a estrutura atômica superficial eo processo de adsorção-dessorção reversível de hidrogênio em eletrodos monocristalinos Pt (111), Pt (100) e Pt (110), Quím. Nova 24 (6) (2001) 856.
[42] E.J. Dickinson, H. Ekström, E. Fontes, Comsol multiphysics®: Finite element software for electrochemical analysis. a mini-review, Electrochem. Commun. 40 (2014) 71–74.
[43] E.B. Carneiro-Neto, M.S. Sikora, E.C. Pereira, M.C. Lopes, Probing the numerical convergence of a commercial finite element software in electrochemical simulations, Electrochemistry (Tokyo, Jpn.) 82 (11) (2014) 966–973.
[44] M. Ciszkowska, A. Jaworski, J. Osteryoung, Voltammetric reduction of hydrogen ion in solutions of polyprotic strong acids with and without supporting electrolyte, J. Electroanal. 423 (1997) 95–101.